Medical applications of shortwave FM radar: Remote monitoring of cardiac and respiratory motion

K. Mostov and E. Liptsen
Systems Micro Technologies, 2614 Warring Street, Suite 3, Berkeley, California 94704

R. Boutchko[a)]
Lawrence Berkeley National Laboratory, 1 Cyclotron Road, M.S. 55R0121, Berkeley, California 94720

(Received 16 June 2009; revised 28 September 2009; accepted for publication 2 November 2009; published 1 March 2010)

Purpose: This article introduces the use of low power continuous wave frequency modulated radar for medical applications, specifically for remote monitoring of vital signs in patients.
Methods: Gigahertz frequency radar measures the electromagnetic wave signal reflected from the surface of a human body and from tissue boundaries. Time series analysis of the measured signal provides simultaneous information on range, size, and reflective properties of multiple targets in the field of view of the radar. This information is used to extract the respiratory and cardiac rates of the patient in real time.
Results: The results from several preliminary human subject experiments are provided. The heart and respiration rate frequencies extracted from the radar signal match those measured independently for all the experiments, including a case when additional targets are simultaneously resolved in the field of view and a case when only the patient's extremity is visible to the radar antennas.
Conclusions: Micropower continuous wave FM radar is a reliable, robust, inexpensive, and harmless tool for real-time monitoring of the cardiac and respiratory rates. Additionally, it opens a range of new and exciting opportunities in diagnostic and critical care medicine. Differences between the presented approach and other types of radars used for biomedical applications are discussed. © *2010 American Association of Physicists in Medicine*. [DOI: 10.1118/1.3267038]

I. INTRODUCTION

Electromagnetic (EM) radar has been used to detect and characterize targets of various nature for almost a century. Most of the early radar development was driven by military applications, with typical operating distances of hundreds of meters or more. Technological progress in the second half of the 20th century enabled new radar applications with target ranges in meters or less; these included biomedical applications first suggested in the late 1970s. Many of the key concepts of biological target detection and microwave imaging, including measurements of dielectric permittivity and conductivity of biological tissues at microwave frequencies, were first systematized in Ref. 1.

During the past decade, two types of radar were applied in the diagnostic medicine: Ultra-wide-band (UWB) and single frequency continuous wave (CW) radar. The proposed UWB applications include the detection of cerebral hematoma,[2] breast cancer,[3] measurement of vital signs, and possible radar tomography.[4] Published implementations of CW radar include Doppler radar[5,6] and phase detecting CW radar.[8–10] Doppler radar is designed for measuring velocity of moving targets, while phase detecting radar can detect small variations in the target range. The scope of constant frequency CW radar applications is mostly limited to respiration and cardiac activity monitoring in a single patient and derivative applications such as detecting subtle changes in cardiac activity caused by stress.[11]

This work focuses on a different type of biomedical radar—continuous wave frequency modulated (FM) radar. The FM radar concept was first proposed in 1928 (Ref. 12) and first adapted in war-time aircraft detection systems. Its applications range from ground-penetrating radars to missile tracking. FM radar application for vital sign detection has been patented as a concept in 1990 (Ref. 14) and briefly discussed in Ref. 13. We have implemented the micropower radar with linear frequency modulation that allows simultaneous acquisition of reflection data for targets located at different ranges from the radar antennas. This approach combines the ranging capabilities of UWB with sensitivity and robustness of Doppler technology. We demonstrate the feasibility of the currently implemented prototype of our radar by applying it for remote monitoring of respiration and cardiac activity, with other potential biomedical applications discussed.

Section II of this paper gives a short description of the proposed technology. Section III describes the first experimental results obtained using our approach, and Sec. IV discusses possible applications of our radar in diagnostic medicine. The attachment provides a brief comparison between our technology and other types of biomedical radar.

II. METHODS

II.A. Radar operation

The operation of EM radar relies on the phenomenon of EM wave reflection by material boundaries. Biological tissues with different dielectric properties[15] form wave-reflecting boundaries in microwave range; for example, our studies confirm that a typical blood-tissue interface reflects up to 10% of the incident signal.

Radar emits a radio-frequency wave S_0 and measures a return signal S_r reflected by one or more objects of interests or *targets*. Target range and scattering cross section are determined by analyzing intensity and phase (and in some applications, polarization and spectral composition) of S_r. Depending on $S_0(t)$, several radar classifications exist, as discussed in the Appendix. This paper focuses on FM continuous wave radar. The basic theory of FM radar operation can be found in a number of standard textbooks, see e.g., Ref. 16. Below, we describe the signal processing aspects of the micropower frequency modulated radar (MFMR) considered in this work.

MFMR consists of neighboring emitter and receiver antennas. The emitter signal S_0 is characterized by its amplitude A and frequency modulation function $F(t)$,

$$S_0 = A\cos\Phi(t), \quad \text{where } \Phi(t) = 2\pi\int_0^t F(t')dt'. \tag{1}$$

This signal is reflected by targets in the field of view of the radar. Let targets be indexed by m and characterized by their range r_m and reflection cross section σ_m. In the first approximation, ignoring multiple reflections, the signal received by the radar $S_r(t)$ would consist of a superposition of reflections from individual targets:

$$S_r = \sum_m A\frac{\mu(r_m)\sigma_m}{(4\pi)^2 r_m^4}\cos\Phi(t-\tau(r_m)).$$

Here, μ is a range-dependent medium attenuation factor and τ or *time of flight* (TOF) is the time of signal propagation from the radar to the target and back. The speed of light c depends on the medium, but in the simplest case of uniform medium,

$$\tau = 2r/c. \tag{2}$$

In general, σ_m depends on a large number of parameters, such as dielectric and magnetic properties of the target and its surrounding, target size, surface roughness, and angle of incidence. We do not consider these factors in detail since our goal is limited to the detection of the presence of intertissue boundaries and determining their spatial positions (as opposed to the much more complex problem of *microwave reflection tomography*, which we do not attempt to solve here). We combine the reflectivity, attenuation, and beam divergence effects into one variable, reflecting strength c_m, specific for each target. This convenience simplifies the above equation to

$$S_r(t) = \sum_m c_m\cos\Phi(t-\tau_m). \tag{3}$$

The main goal of radar sensing is measuring c_m and τ_m for the targets of interest. Specific properties of the targets and their environment are established during subsequent analysis and interpretation of $c_m(\tau_m)$ information.

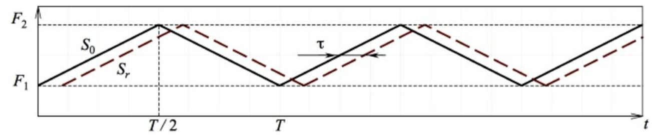

FIG. 1. Frequency modulation function. The solid line denotes the instantaneous frequency of the emitted signal (1) and the dashed line that of a signal reflected by a target with time of flight τ.

Different types of frequency modulation functions $F(t)$ and corresponding processing methods have been considered over time in FM radar applications. We propose to use a symmetric (isosceles) linear modulation function, shown in Fig. 1, with $F_1 = 10$ GHz and $F_2 = 11$ GHz, and $1/T = 55$ kHz. In this application, we only use the up-slope portion of $F(t)$. Since typical TOF values are below 20–30 ns, and reflections from targets with $\tau > 1$ μs can be neglected because of dispersion and attenuation effects, we treat F as a linear function of time defined on $t \in \{0, T/2\}$. Phase Φ of the emitted signal then depends on time quadratically,

$$\Phi(t) = 2\pi\left\{F_1 t + \frac{\Delta F}{T}t^2,\right\}, \quad \text{where } \Delta F = F_2 - F_1. \tag{4}$$

II.B. Signal processing

It is convenient to represent the distribution of the targets as a continuous function of time of flight and, therefore, range. Let

$$C(\tau)d\tau = \sum_m c_m, \quad \tau \leqslant \tau_m < \tau + d\tau. \tag{5}$$

This allows us to rewrite expression (3) for the incoming signal as an integral,

$$S_r(t) = A\int_0^\infty C(\tau)\cos\Phi(t-\tau)d\tau. \tag{6}$$

As we have mentioned above, $C(\tau)$ vanishes for $\tau > 1$ μs; hence, it is safe to adopt infinite integration limits while retaining approximate equation for phase (4). A target (reflecting boundary) at TOF τ_o creates a local maximum of $C(\tau)$ at $\tau = \tau_o$. Signal processing needed to find $C(\tau)$ is organized in four stages.

(1) Initial processing is implemented using analog components of the radar circuit. First, the received signal (6) is multiplied by the currently emitted signal and scaled,

$$S_r(t) \to \frac{2}{A^2}\cos\Phi(t)S_r(t)$$
$$= \int_0^\infty C(\tau)2\cos\Phi(t)\cos\Phi(t-\tau)d\tau. \tag{7}$$

The product of two cosines in the integrand can be transformed to a sum

$$2\cos\Phi(t)\cos\Phi(t-\tau) = \cos[\Phi(t)+\Phi(t-\tau)] + \cos[\Phi(t)-\Phi(t-\tau)], \quad (8)$$

where the instantaneous oscillation frequency of the first term is at least $2F_1 = 20$ GHz or more. This rapidly oscillating term is removed by an analog low-pass filter. After the filtration, taking into account Eq. (4) and neglecting small $\sim\tau^2$ terms, we can rewrite the modified received signal as $S_r(t)$,

$$\hat{S}_r(t) = \int_0^\infty C(\tau)\cos 2\pi\left(\frac{2\Delta F t}{T}\tau + F_1\tau\right)d\tau. \quad (9)$$

(2) On the output of the analog part of radar circuit board, signal (9) represents a cosine part of the Fourier transform of $C(\tau)$ with a phase shift $\Delta\theta = F_1\tau$. This signal is digitized as 1024 samples on $\{0, T/2\}$ and transformed using a hardware-implemented fast Fourier transform (FFT) algorithm. The results of FFT is a sequence of complex values of $C_k \equiv C(\tau_k)$. C_k is related to individual target reflection strength c_m as

$$C_k = \sum c_m(\tau_m), \quad \tau_m \in \{\tau_k \pm \Delta\tau/2\}, \quad \tau_k = k\Delta\tau. \quad (10)$$

Real and imaginary parts of C_k are transferred to a computer with the read-out frequency of 120 Hz. Theoretically, read-out frequency can be as high as $1/T = 55$ kHz; however, its current value is limited by the hardware performance.

(3) The physical meaning of $\mathrm{Re}(C_k)$ and $\mathrm{Im}(C_k)$ is best seen in a polar representation. For each value of τ_k, we compute the *amplitude*

$$A_k \equiv A(\tau_k) = \sqrt{[\mathrm{Re}(C_k)]^2 + [\mathrm{Im}(C_k)]^2} \quad (11)$$

and the *phase*

$$\theta_k \equiv \theta(\tau_k) = \tan^{-1}\left\{\frac{\mathrm{Im}(C_k)}{\mathrm{Re}(C_k)}\right\} = 2\pi F_1\tau. \quad (12)$$

The amplitude (11) describes the net reflective strength of all targets in the radar field of view with time of flight in the interval $\{\tau_k \pm \Delta\tau/2\}$, and the phase (12) provides a more sensitive measure of the mean τ to the targets in this interval. The inverse FFT of Eq. (9) is band limited at $t = T/2$, which defines the resolution of the TOF interval

$$\Delta\tau = \frac{1}{F_2 - F_1} = 1 \text{ ns}. \quad (13)$$

This value of $\Delta\tau$ translates to range resolution $\Delta r = 15$ cm in air and less in media with smaller speed of light. Within each τ_k interval, the mean target range can be computed with much higher precision using Eq. (12). MFMR prototype hardware allows measuring θ_k with 10° precision, which translates to 0.5 mm range resolution. Since maximum change in τ computable from Eq. (12) is $\sim\Delta\tau/20$ (this corresponds to 180° phase change), the phase measurement cannot be used to determine the *absolute* range. Therefore, we distinguish two different range resolution measures: 15 cm range difference between targets is necessary to resolve them from a single radar reflection data set and 0.5 mm is the minimum change in the individual target range that can be detected with time.

(4) $\mathrm{Re}(C_k)$ and $\mathrm{Im}(C_k)$ arrays are read by the attached computer console and converted to A_k and θ_k sequences in real time. During the next step, we isolate the τ_k interval of interest. If the patient is the only moving object in the field of view, then the value of k' that corresponds to the maximum variance of $A_k(t)$ is selected. Otherwise, if the radar "sees" additional persons or moving objects, k' is selected manually. In the subsequent analysis, time series $A_{k'}(t)$ and $\theta_{k'}(t)$ are band filtered to suppress noise and to amplify the type of motion of interest to us. Postprocessing time series analysis of $A_{k'}$ and $\theta_{k'}$ consists of the digital Fourier transform of 120 Hz sampled data and several band-filtering stages needed to amplify either respiratory or cardiac motion. Typically, respiratory motion filter zeroes signal components outside the 0.05–0.6 Hz window, the cardiac window is 0.6–4 Hz. Numerical values of heart rate and respiration rate are determined by the spectral analysis as the maxima of the frequency distributions of the appropriately band-filtered signals.

III. EXPERIMENTAL RESULTS

A micropower FM radar prototype has been built by our group at Systems Micro Technologies (http://www.sysmicrotech.com). Table I shows the technical characteristics of the prototype acquisition unit, which contains radar antennas, and electronics components that perform processing steps (1) and (2) from Sec. II B. Subsequent processing is performed on an attached computer. In the future, we plan to integrate the acquisition, data processing, and user interface hardware into one miniature unit.

Three sets of human subject experiments have been conducted using the MFMR prototype in order to validate its ability to measure heart rate and monitor respiration. The prototype was placed two meters from the human subject,

TABLE I. MFMR prototype characteristics. Low radiated power means that signal power density at distances 30 cm or more is below 1 μW/cm^2, which is typical to common household appliances and does not pose significant health risks (Ref. 17).

Prototype size	$15\times10\times5$ cm^3
Antenna bandwidth	10–11 GHz
Data sampling rate	120 Hz
Radiated power	0.8 mW
Measurement range	0.5–10 m
Field of view	50°
Range resolution[a]	0.5 mm
Target resolution[b]	15 cm

[a]Minimum detectable change in the target range.
[b]Minimum resolvable distance between individual targets.

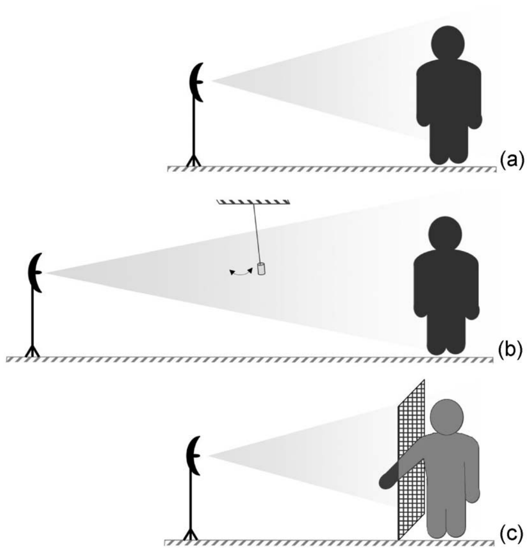

FIG. 2. Setup of the human subject experiments. (a) Measuring (constant) breathing and cardiac rates from signal reflected by the patient's chest. (b) Measuring two targets simultaneously: A small ceramic pendulum is placed halfway between the radar and the subject. (c) Monitoring uneven respiration using signal reflected by the patient's hand. The rest of the patient's body is shielded by a 1 mm fine copper mesh screen.

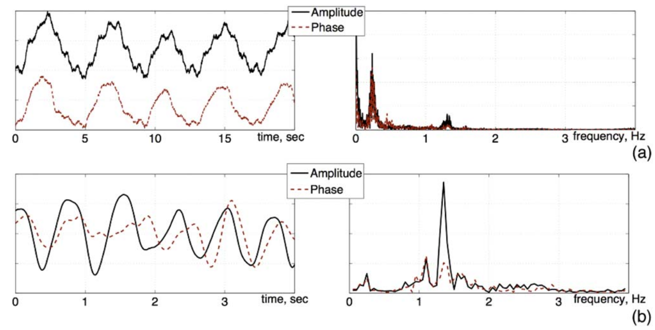

FIG. 3. Amplitude and phase shift of effective radar cross section of a human subject, proportional units. Left: time-domain plots. Right: Frequency-domain plots. (a) Respiration-filtered signal. 0.25 Hz peaks in both amplitude and phase frequency curves correspond to 15 breaths per minute. (b) Cardiac-filtered radar data. Frequency peaks at 1.3 Hz correspond to the heart rate of 78 bpm. Note the shorter time-domain display window: 0–4 s.

the reflection data were collected for 1 min and processed following the procedure described in Sec. II B. In order to optimize the display of the results, additional scaling has been imposed on the radar data.

In the first experiment shown in Fig. 2(a), MFMR beam was centered on the subject's chest. Respiratory and cardiac rates were measured simultaneously using both the radar and an independent method. The heartrate of 78 beats per minute (bpm) was measured using a standard pulse oximeter. The rate of controlled breathing was 15 bpm, verified by a Vernier respiration monitor belt (http://www.vernier.com/probes/rmb.html). In Fig. 3, we show both time-domain and frequency-domain results of A and θ for this experiment. The respiratory rate was determined to be 4 s/breath or 15 bpm from the 0.25 Hz peak in the Fig. 3(a) plot. The cardiac frequency of 1.3 Hz corresponds to the 78 bpm rate measured by the blood oximeter.

Experiment shown in Fig. 3(b) was designed to validate MFMR ability to characterize more than one target from a single measurement. The previous experiment was modified by adding a pendulum at 1 m range from the radar antennas. The pendulum, made from a 2-cm-wide and 5-cm-long ceramic cylinder suspended on a string, oscillated at 27 bpm. Amplitude series $A_k(t)$ for different values of k corresponding to 1 and 2 m ranges have been analyzed to compute the pendulum oscillation frequency (0.45 Hz or 27 bpm), human subject's mean respiration rate (21 bpm) and heartrate (98 bpm). Independently measured respiratory rate and heartrate for the human were respectfully 20 and 96 bpm. In Fig. 4(a), we show a 9 s interval of the radar amplitude components corresponding to the pendulum location and to the human subject location. The 2.22 s pendulum oscillations are clearly identifiable (the higher-frequency components correspond to other oscillatory degrees of freedom such as rotation of the ceramic cylinder about its horizontal axes). Both cardiac motion and respiratory motion are identifiable on the amplitude curves for the human subject-reflected signal.

The goal of the experiment shown in Fig. 2(c) was to test MFMR sensitivity to weak signals, namely, radar reflection from the patient's extremity only. The subject's torso, head and legs were screened from the radar by a conducting copper mesh with 1 mm spacing so that only a forearm and a

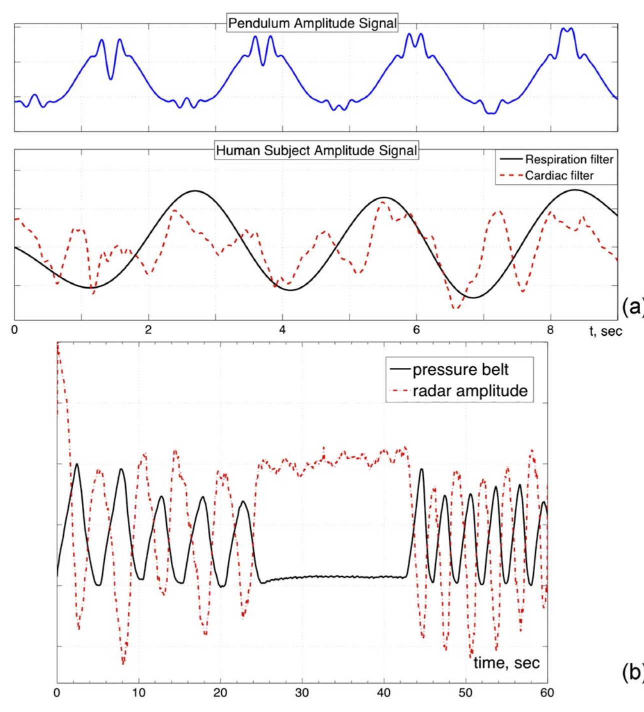

FIG. 4. All plots use arbitrary units. (a) MFMR used to measure the patient's vital signs and the oscillation frequency of a pendulum. Top: Denoised pendulum signal, A_{10} (frequencies above 6 Hz cut off). Bottom: Human subject signal A_{20} filtered to amplify respiration (0.01–0.6 Hz band filter) and cardiac motion (0.6–6 Hz band filter). (b) Radar reflection off the subject's hand vs pressure belt signal. Coached breathing pattern: five deep breaths at 5 s/cycle, a 18 s breathhold, six breaths at 3 s/cycle. The signals derived from the radar and from the respiration monitor belt clearly mirror each other.

hand were "visible" to the antennas. The subject was instructed to breathe following a specific pattern: Five 5 s breaths, one 18 s breath-hold, and then six 3 s breaths, the breathing pattern was verified using the Vernier respiration monitor belt. In Fig. 4(b) we show time curves for both the belt and MFMR's amplitude. Both the air-pressure belt and the MFMR signals exhibit the same time dependence up to a scaling factor, confirming that the MFMR can be used to follow respiratory activity in real time even if the direct view of patient's chest is obstructed.

IV. DISCUSSION

The results of the validation experiments confirm that the micropower FM radar technology implemented by SMT can be used to measure human heart rate and respiration rate. Large-scale patient studies are needed to quantify the precision of our approach. Like other continuous wave radar technologies discussed in the attachment, MFMR uses time series analysis of the radar reflection patterns to resolve the two types of motion. The main innovative aspect of MFMR in comparison to other reported radars is the combination of range resolution capability and the high sensitivity of the new technology. Spatial resolution currently achieved in MFMR prototype matches that of most UWB radars with an added benefit of simultaneous acquisition of reflection patterns from a large interval of different ranges. High sensitivity displayed by MFMR has been reported previously in phase-detecting single frequency CW radars such as in Ref. 8. However, single frequency radar is also sensitive to signal contamination caused by reflection from other moving objects or people. Potentially, MFMR may prove to be more reliable when used in suboptimal environment like hospital wards and waiting rooms.

One of the most interesting results presented in Sec. III is the experiment displayed in Fig. 2(c). Remote vital signs monitoring conducted from a single extremity observation can be useful in many potential MFMR applications. At this point, the exact explanation of how the radar cross section of an extremity is connected to respiration has not been confirmed. The most likely mechanism is a combination of two factors. The dominant factor is the effect of micromovements of the subject's limbs or clothes induced by breathing. In addition to that, MFMR may detect small changes in the blood flow regulated by the changes in blood oxygenation caused by respiration. Establishing this response mechanism and relating radar signal to blood flow in different organs is one of the main directions of our current research.

A multitude of medical applications can be suggested for the device presented in our work. The simplest type of an application is quick remote measurement of heart and respiratory rates in both clinical and nonclinical environment. This application yields several potential benefits such as increased convenience for patients and hospital staff, shorter patient visit time, fewer procedures that require direct patient-staff interaction, and reduced likelihood of human error in measuring and recording vital signs information. Upon achieving more reliable measurement results, additional applications that target specific patient conditions such as sleep apnea or cardiac arrhythmia can be proposed.

Another immediate targeted MFMR application is to provide respiratory gating information for motion compensation during different types of medical imaging scans, such as PET, SPECT, or x-ray CT or during radiation therapy. Currently used methods of motion monitoring are frequently inconvenient to patients and demanding of hospital staff. Our radar will enable real-time respiratory gating without the need for any probes or electrodes connected to the patient.

FM radar spatial resolution and time resolution strongly depend on the hardware specifications. While our theoretical results rely on the fact that the frequency modulation function matches that in Fig. 1, achieving high-quality linear FM signal in the GHz range and validating its correspondence to the etalon is extremely hard. Currently, both the linearity of FM function and its bounds F_1 and F_2 are determined only approximately. FM function nonlinearity degrades the range resolution by causing spill-over between neighboring values of radar cross-sectional components $C(\tau_k)$. Other hardware imperfections include high level of electronic noise, and cross-talk between the emitter and receiver antennas. Electronic noise lowers the overall signal-to-noise ratio of the prototype. Antenna cross-talk causes the "dead-zone" artifact, a strong phantom signal for range values less than 1 m. Overall, present MFMR specifications are still below their theoretically achievable limits.

In addition to hardware improvement, an important part of MFMR research is directed at formulating a complete model of FM radar performance. Historically, radar theory has been developed and perfected for ranges much larger than either the target size or the base radar wavelength. Current mathematical description, both provided in Sec. II and in the referenced literature, is approximate and makes a number of assumptions. While the overall model is generally valid and confirmed by experiments, we are still working on formulating the exact forward problem of radar propagation: a framework that would predict the measured reflection pattern for a known target distribution. This model is essential in the development of efficient signal artifact compensation algorithms.

The introduction of FM radar technology to medicine opens a wide range of research possibilities in hardware development and in the development of new data processing algorithms needed to improve the reliability of measurements and to expand the functionality of radar-based tools.

V. SUMMARY

A new type of GHz-range low-power radar is suggested for medical use. Early experiments in a controlled environment confirm the ability of the device to obtain simultaneous measurements of both respiration and heart rates without any physical contact between the patient and the device. MFMR exhibits both high signal sensitivity and good range resolution. Several clinical applications are suggested for the new device.

ACKNOWLEDGMENTS

Experimental, theoretical, and research works on the MFMR technology described in this paper was supported by Systems Micro Technologies, Kirsen Medical Technology, and Kirsen Technologies capital, as well as private investments. The theoretical and research work of Dr. Boutchko related to respiratory gating and other related aspects were supported in part by the National Institutes of Health of the U.S. Department of Health and Human Services under Grant Nos. R01-EB00121 and R01-HL71253 and by the Director, Office of Science, Office of Biological and Environmental Research of the U.S. Department of Energy under Contract No. DE-AC02-05CH11231. The authors would like to thank Dr. Grant Gullberg for useful suggestions and for providing the Jaszczak dynamic cardiac phantom for early experiments, and Dr. Thomas Budinger and Dr. Eugene Mishchenko for helpful discussions.

APPENDIX: OPERATIONAL PRINCIPLES OF OTHER RADARS

Below, we summarize some of the basic principles of radar operation and explain the difference between pulse radar and single or modulated frequency continuous wave radar. The purpose of this attachment is to help a reader new to the field to understand the optimal applications and intrinsic limitations of different radar types.

Using the same notations as in Sec. II, we distinguish radar types based on the functional form of the emitted signal $S_0(t)$. Amplitude and frequency parameters of $S_0(t)$ define the signal processing methods needed to extract target information from the reflected signal $S_r(t)$.

In pulse or ultra-wide-band (UWB) radar $S_0(t)$ represents a series of short, $t_{\text{pulse}} \sim 1$ ns, pulses of radiation, emitted every t_{repeat}, usually much greater than t_{pulse} in order to accommodate expected target TOF. Frequency distribution of each pulse is typically very wide, $\sim 0.1-100$ GHz, hence the UWB term. After a pulse is emitted, the radar waits fixed time τ and computes the amplitude of the received pulse. By varying τ, a complete measurement of $C(\tau)$ as defined in Eq. (5) can be obtained. This approach is effective in applications where the main goal is measuring the target range. The downside of UWB radar is the fact that since $t_{\text{pulse}} \ll t_{\text{repeat}}$, time-averaged radiation power and, consequently, effective sensitivity of the technology is lower than in CW radar. Increasing pulse amplitude is not always feasible because radar peak signal intensity is constrained by safety regulations.[17] Range resolution of UWB radar is also limited by the pulse width, and available resolution-improving methods are typically accompanied by significant increases in the size of UWB radar units. For example, the subcentimeter resolution claimed by Li *et al.* in Ref. 3 is only possible when a single receiver antenna is substituted by an antenna array.

In single-frequency continuous wave (SF CW) radar, $S_0 = A\cos\omega t$, where the frequency ω is constant. The reflected signal is similar to Eq. (3). If C_m denotes collective reflection and attenuation property of the m_{th} target, τ_m denotes the time of flight for that target, and $v_{m,r}$ denotes the radial component of its velocity, then

$$S_r(t) = \sum_m C_m \cos\left[\omega\left(1 - \frac{v_{m,r}}{c}\right)t - \omega\tau_m\right].$$

The Doppler frequency shift is extracted from $S_r(t)$ and used to study the moving targets. This approach is rather straightforward, however, less sensitive to small-scale slow motion such as the motion of human heart. In phase-detecting SF CW radar such as in Ref. 7, as well as in MFMR, Doppler effect is neglected as second order. Instead, if $S_r(t)$ is Fourier transformed and subjected to a series of transformations similar to those described in Sec. II B, the resulting signal becomes

$$\hat{S}_r = \sum_m C_m \cos(\omega\tau_m).$$

If the m_{th} target moves so that τ_m varies with time, frequency characteristics of this motion can be obtained by time series analysis of $\hat{S}(t)$. Since, typically, $\tau \gg 1/F$ only the change in τ_m can be measured, while the absolute value of τ_m remains unknown. Most importantly, if several targets move simultaneously, frequency analysis alone may be insufficient to resolve motion of the individual targets. While in MFMR, the amplitude (11) and phase (12) of different C_k from (10) are analyzed individually, single frequency radar analyzes a quantity similar to $\Sigma_k C_k$. Alternatively, one may view SF CW radar as a subset of MFMR with $\Delta\tau \to \infty$. In this case, it is easy to see a scenario when the motion of interest is masked by other targets.

Finally, a different approach to frequency modulated CW radar is suggested in Ref. 13. There, time-dependent instant phase function $\Phi(t)$ is assumed. The authors propose to filter $S_r(t)$ against $\cos\Phi(t-\tau_o)$ for fixed τ_o. The goal is to isolate the portion of the received signal that corresponds to targets with $\tau \sim \tau_o$. To the best of our understanding, this interesting idea has not been implemented in practice yet, so we cannot compare the details of its performance to our approach.

[a]Electronic mail: rbuchko@lbl.gov

[1]*Medical Applications of Microwave Imaging*, edited by L. E. Larsen and J. H. Jacobi (IEEE, Piscataway, NJ, 1986).

[2]W. S. Haddad, J. E. Trebes, and D. L. Matthews, "Microwave hematoma detector," U.S. Patent No. 6,233,479 B1 (15 May 2001).

[3]X. Li, E. J. Bond, B. D. Van Veen, and S. C. Hagness, "An overview of ultrawideband microwave imaging via space-time beamforming for early-stage breast cancer detection," IEEE Antennas Propag. Mag. **47**, 19–34 (2005).

[4]E. M. Staderini, "UWB radars in medicine," IEEE Aerosp. Electron. Syst. Mag. **17**(1), 13–18 (2002).

[5]B. Lohman, O. Boric-Lubecke, V. M. Lubecke, P. W. Ong, and M. M. Sondhi, "A digital signal processor for Doppler radar sensing of vital signs," Med. Biol. Eng. Comput. **21**, 161–164 (2002).

[6]A. Host-Madsen, N. Petrochilos, O. Boric-Lubecke, V. M. Lubecke, B.-K. Park, and Q. Zhou, "Signal processing methods for Doppler radar heart rate monitoring," in *Signal Processing Techniques for Knowledge Extraction and Information Fusion*, edited by D. Mandic, M. Golz, A. Kuh, D. Obradovic, and T. Tanaka (Springer, New York, 2008), pp. 121–140.

[7]H. J. Kim, K. H. Kim, Y. S. Hong, and J. J. Choi, "Measurement of human heartbeat and respiration signals using phase detection radar," Rev. Sci. Instrum. **78**, 104703-1–104703-3 (2007).

[8]M. Varanini, P. C. Berardi, F. Conforti, M. Micalizzi, D. Neglia, and A. Macerata, “Cardiac and respiratory monitoring through non-invasive and contactless radar technique,” Comput. Cardiol. **35**, 149–152 (2008).
[9]C. Li, Y. Xiao, and J. Lin, “Experiment and spectral analysis of a low-power Ka-band heartbeat detector measuring from four sides of a human body,” IEEE Trans. Microwave Theory Tech. **54**(12), 4464–4471 (2006).
[10]D. Dei, G. Grazzini, G. Luzi, M. Pieraccini, C. Atzeni, S. Boncinelli, G. Camiciottoli, W. Castellani, M. Marsili, and J. Lo Dico, “Non-contact detection of breathing using a microwave sensor,” Sensors **9**, 2574–2585 (2009).
[11]S. Suzuki, T. Matsui, H. Imuta, M. Uenoyama, H. Yura, M. Ishihara, and M. Kawakami, “A novel autonomic activation measurement method for stress monitoring: Non-contact measurement of heart rate variability using a compact microwave radar,” Med. Biol. Eng. Comput. **46**, 709–714 (2008).
[12]J. O. Bentley, “Airplane altitude indicating system,” U.S. Patent No. 2,011,392 (13 August 1935).
[13]G. Matthews, B. Sudduth, and M. Burrow, “A non-contact vital signs monitor,” Crit. Rev. Biomed. Eng. **28**(1–2), 173–178 (2000).
[14]S. M. Sharpe, J. Seals, A. H. MacDonald, and S. R. Crowgey, “Non-contact vital signs monitor,” U.S. Patent No. 4,958,638 (September 25, 1990).
[15]J. C. Lin, “Microwave propagation in biological dielectrics with application to cardiopulmonary interrogation,” *Medical Applications of Microwave imaging* (Ref. 1), pp. 47–58.
[16]I. V. Komarov, S. M. Smolskiy, and D. K. Barton, *Fundamentals of Short-Range FM Radar*, translated by D. K. Barton (Artech House, Boston, 2003).
[17]R. F. Cleveland, Jr. and Jerry L. Ulcek, *Questions and Answers about Biological Effects and Potential Hazards of Radiofrequency Electromagnetic Fields*, OET Bulletin No. 56, Fourth Edition (Office of Engineering and Technology Federal Communications Commission Washington, DC 20554, August 1999).